

Article

Thermodynamic Assessment of the P_2O_5 - Na_2O and P_2O_5 - MgO Systems

Lideng Ye¹, Chenbo Li¹, Jifeng Yang¹, Guangcheng Xiao¹, Zixuan Deng¹, Libin Liu¹, Ligang Zhang^{1,*} and Yun Jiang^{2,*}

¹ School of Material Science and Engineering, Central South University, Changsha 410083, China

² NMPA Key Laboratory for Pharmaceutical Excipients Engineering Technology Research, Hunan Institute for Drug Control, Changsha 410001, China

* Correspondence: ligangzhang@csu.edu.cn (L.Z.); jiangyun127@hotmail.com (Y.J.);
Tel.: +86-182-2949-3731 (L.Z.); +86-0731-8887-7732 (Y.J.)

Abstract: Knowledge about the thermodynamic equilibria of the P_2O_5 - Na_2O and P_2O_5 - MgO systems is very important for controlling the phosphorus content of steel materials in the process of steelmaking dephosphorization. The phase equilibrium and thermodynamic data of the P_2O_5 - Na_2O and P_2O_5 - MgO systems were critically evaluated and re-assessed by the CALPHAD (Calculation of PHase Diagram) approach. The liquid phase was described by the ionic two-sublattice model for the first time with the formulas $(Na^{+1})_P(O^{-2}, PO_3^{-1}, PO_4^{-3}, PO_{5/2})_Q$ and $(Mg^{+2})_P(O^{-2}, PO_3^{-1}, PO_4^{-3}, PO_{5/2})_Q$, respectively, and the selection of the species constituting the liquid phase was based on the structure of the phosphate melts. A new and improved self-consistent set of thermodynamic parameters for the P_2O_5 - Na_2O and P_2O_5 - MgO systems was finally obtained, and the calculated phase diagram and thermodynamic properties exhibited excellent agreement with the experimental data. The difference in the phase composition of invariant reactions from the experimentally determined values reported in the literature is less than 0.9 mol.%. The present thermodynamic modeling contributes to constructing a multicomponent oxide thermodynamic database in the process of steelmaking dephosphorization.

Keywords: P_2O_5 - Na_2O system; P_2O_5 - MgO system; CALPHAD; thermodynamic optimization; phase diagram



Citation: Ye, L.; Li, C.; Yang, J.; Xiao, G.; Deng, Z.; Liu, L.; Zhang, L.; Jiang, Y. Thermodynamic Assessment of the P_2O_5 - Na_2O and P_2O_5 - MgO Systems. *Materials* **2024**, *17*, 2221. <https://doi.org/10.3390/ma17102221>

Academic Editor: Neven Ukrainczyk

Received: 26 March 2024

Revised: 16 April 2024

Accepted: 30 April 2024

Published: 8 May 2024



Copyright: © 2024 by the authors. Licensee MDPI, Basel, Switzerland. This article is an open access article distributed under the terms and conditions of the Creative Commons Attribution (CC BY) license (<https://creativecommons.org/licenses/by/4.0/>).

1. Introduction

As society progresses, industries advance to higher developmental stages, leading to more demanding usage of steel materials and increased quality requirements for steel materials across various sectors. Phosphorus, as one of the detrimental elements in steel, serves as a critical indicator of steel quality. Therefore, the control of phosphorus content in steel remains a crucial target for enterprise development. In the steelmaking process, the inclusion of alkaline earth metal oxide fluxes such as MgO can effectively diminish phosphorus in liquid steel, while alkali metal oxide fluxes like Na_2O also exhibit a strong dephosphorization effect [1]. The phase diagrams and thermodynamic properties of the P_2O_5 - Na_2O and P_2O_5 - MgO systems are essential to effectively control the dephosphorization effect of slags and to understand the phosphorus distribution ratio between liquid iron and oxide slags such as Na_2O and MgO . Furthermore, good thermodynamic descriptions provide phase diagrams and thermodynamic data that can also effectively provide a theoretical basis for material design [2–6].

Xie et al. [7] utilized the modified quasi-chemical model to describe the liquid phase and firstly optimized the thermodynamic parameters of the P_2O_5 - Na_2O system based on the reliable experimental phase diagram and thermodynamic properties, and their calculations were in good agreement with the experimental data, while the description of the enthalpy of formation of $Na_5P_3O_{10}$ was inaccurate. In 2015, Ding et al. [8] evaluated

a P_2O_5 -MgO system by using the modified quasi-chemical model to describe the liquid phase, and PO_4^{3-} was considered the basic unit of P_2O_5 in the liquid phase, but the calculations showed significant discrepancies with the experimental data. Furthermore, a set of thermodynamic data describing the liquid phase with the modified quasi-chemical model does not simultaneously describe both the oxide and metal liquid phases, which limits the study of the phosphorus distribution ratio between liquid iron and oxide slags. Therefore, it is meaningful to construct a set of multicomponent thermodynamic databases that can describe both oxide and metal liquids using appropriate thermodynamic models to guide the addition of oxide fluxes in the steelmaking dephosphorization process. The ionic two-sublattice model allowing one set of the thermodynamic parameters to simultaneously describe both the oxide and metallic liquid [9] was used to describe the liquid phase for the first time in the current work. Additionally, the ionic two-sublattice model can not only rationally describe the phosphate melt structure but also adequately reproduce the thermodynamic properties of complex liquids such as slag [10,11]. This is highly beneficial to the construction of a slag system multivariate database to guide steelmaking dephosphorization.

This work aimed to conduct a phase diagram thermodynamic optimization of the P_2O_5 - Na_2O and P_2O_5 -MgO systems using the CALPHAD (CALculation of PHase Diagram) approach through establishing suitable thermodynamic models. The crystal structure, limited measured phase diagram and thermodynamic properties were optimized to construct a Gibbs energy expression for each phase in the systems to obtain a set of thermodynamic parameters reasonably describing the phase diagrams, covering the whole composition range using Thermo-Calc software.

2. Review of Literature Data

The experimental phase diagram information and thermodynamic property data of the P_2O_5 - Na_2O and P_2O_5 -MgO systems are systematically evaluated. The crystal structures of the solid phases in the systems are listed in Table 1.

Table 1. Crystal structures of all solid phases in the P_2O_5 - Na_2O and P_2O_5 -MgO systems.

System	Compound	Crystal System	Space Group	Reference
P_2O_5 - Na_2O	γ - $NaPO_3$	Orthorhombic	$P2_1P2_1P2_1$	[12]
		Orthorhombic	$Pnma$	[13]
	β - $NaPO_3$	Triclinic	$P2_1/n$	[14]
		α - $NaPO_3$	Monoclinic	$P2_1/c$
	β - $Na_5P_3O_{10}$	Monoclinic	$C2/c$	[16]
	α - $Na_5P_3O_{10}$	Monoclinic	$C2/c$	[17]
	α - $Na_4P_2O_7$	Orthorhombic	$P2_1P2_1P2_1$	[18]
	β - Na_3PO_4	Tetragonal	$P4_21c$	[19]
	α - Na_3PO_4	Cubic	$Fm\bar{3}m$	[20]
	P_2O_5 -MgO	$Mg_3P_2O_8$	Orthorhombic	$Pnma$
Monoclinic			$P2_1/b$	[22]
Monoclinic			$P2_1/n$	[23]
Monoclinic			$P2_1/n$	[24]
Monoclinic			$P2_1/n$	[25]
β - $Mg_2P_2O_7$		Triclinic	$P\bar{1}$	[26]
		Monoclinic	$P2_1/c$	[27]
		α - $Mg_2P_2O_7$	Monoclinic	$C2/m$
MgP_2O_6		Monoclinic	$C2/c$	[29]
		Monoclinic	$C2/c$	[30]
MgP_4O_{11}		Monoclinic	$P2_1/c$	[31]
		Monoclinic	$P2_1/c$	[32]
		Orthorhombic	$Pmc2_1$	[33]

$\alpha/\beta/\gamma$: the polymorph from high temperature to low temperature.

2.1. P_2O_5 - Na_2O System

A phase diagram of the P_2O_5 - Na_2O system has been reported by several researchers [34–39]. Partridge et al. [34], using thermal, microscopic and X-ray diffraction (XRD) analysis, determined the liquidus of the $NaPO_3$ - $Na_4P_2O_7$ system and confirmed the presence of the $Na_5P_3O_{10}$ compound. Two invariant reactions of $L = \beta - NaPO_3 + \alpha - Na_5P_3O_{10}$ and $L + \alpha - Na_4P_2O_7 = \alpha - Na_5P_3O_{10}$ were reported to occur at 824 K and 893 K, respectively. And the melting points of $NaPO_3$, $Na_5P_3O_{10}$ and $Na_4P_2O_7$ were 898 K, 788 K and 1258 K, respectively. In their work [34], the $Na_4P_2O_7$ and $NaPO_3$ phases exhibited a lot of phase transitions from room temperature to melting point. The transition temperatures of $Na_4P_2O_7$ were found to be 673 K, 783 K, 793 K and 818 K by differential thermal analysis (DTA). Two phase transitions of $NaPO_3$ at 677 K and 783 K were detected. Subsequently, Morey and Ingerson [35] also studied the phase equilibria of the $NaPO_3$ - $Na_4P_2O_7$ system in good agreement with the work of Partridge et al. [34]. Two invariant reactions $L = \beta - NaPO_3 + \alpha - Na_5P_3O_{10}$ and $L + \alpha - Na_4P_2O_7 = \alpha - Na_5P_3O_{10}$ were measured to have reaction temperatures of 825 K and 895 K, and the melting points of $NaPO_3$ and $Na_4P_2O_7$ were observed to be 901 K and 1262 K, respectively, but the third structure of $NaPO_3$ was not found. Turkdogan et al. [36], using the thermal, microscopic, and DTA methods, determined the phase diagram of the $NaPO_3$ - Na_3PO_4 system and did not report the presence of $Na_5P_3O_{10}$. Three invariant reaction temperatures of $L = \beta - NaPO_3 + \alpha - Na_5P_3O_{10}$, $L + \alpha - Na_4P_2O_7 = \alpha - Na_5P_3O_{10}$ and $L = \alpha - Na_4P_2O_7 + \beta - Na_3PO_4$ in the $NaPO_3$ - Na_3PO_4 system were suggested to be 763 K, 893 K and 1218 K by Markina et al. [37], respectively. In 1970, Osterheld et al. [38] determined the phase transition temperature of the $Na_4P_2O_7$ - Na_3PO_4 system below 1573 K by thermal analysis and high-temperature microscopy. They reported that the eutectic reaction $L = \alpha - Na_4P_2O_7 + \beta - Na_3PO_4$ occurred at 1225 K, and two compounds ($Na_4P_2O_7$ and Na_3PO_4) melted congruently at 1271 K and 1785 K, respectively. In 1972, Berak et al. [39] observed three invariant reactions in the liquidus study of the Na_2O - P_2O_5 system. The liquidus data obtained from these works for the P_2O_5 - Na_2O system were in reasonable agreement and were used in the optimization process of the current work. The four compounds $NaPO_3$, $Na_5P_3O_{10}$, $Na_4P_2O_7$ and Na_3PO_4 have polymorphic phase transitions, and the thermodynamic description of the phase transition of the compounds in the P_2O_5 - Na_2O system by Xie et al. [7] based on the reliable literature is more complete, which was considered in the thermodynamic assessment of the present work with refinement and improvement. It is worth noting that there is less information about the experimental phase relation of the P_2O_5 -rich and Na_2O -rich regions in the P_2O_5 - Na_2O system, which still needs to be further determined experimentally.

In 1909, Mixer [40] determined the enthalpy of formation of $NaPO_3$ from its elements using solution calorimetry (SCA). In 1967, Irving et al. [41] also utilized SCA to measure the enthalpy of formation of Na_3PO_4 from its elements at 298 K. Subsequently, in 1968, Irving et al., [42,43] Krivtsov et al., [44] and Zhuang et al. [45] determined the enthalpies of formation of $Na_4P_2O_7$, $Na_5P_3O_{10}$ and $NaPO_3$ from their elements using the SCA method. In 2011, Khaled et al. [46] measured the standard enthalpy of formation of $Na_4P_2O_7$ from its elements using the SCA method. These experimental results were incorporated into the present study with consideration for possible error margins. Andon et al. [47] determined the heat capacities of $NaPO_3$, $Na_5P_3O_{10}$, $Na_4P_2O_7$ and Na_3PO_4 using adiabatic calorimetry within the temperature range of 10 to 320 K. Ashcroft et al. [48] measured the heat capacities of $Na_4P_2O_7$ and $NaPO_3$ from 298 to 620 K and determined the low-temperature transition enthalpy of $Na_4P_2O_7$. Lazarev et al. [49] used DSC to measure the heat capacity of $Na_4P_2O_7$ in the temperature range from 300 to 1000 K and measured the low-temperature enthalpy of transition of the $Na_4P_2O_7$. Grantscharova et al. [50] used DSC to determine the heat capacity of $NaPO_3$ between 468 and 675 K, but their measurements were much higher than those reported by Ashcroft et al. [48]. Considering the above-reported heat capacity data, the data reported by Andon et al. [47], Ashcroft et al. [48] and Lazarev et al. [49] were considered in the present work to optimize the heat capacities of $Na_4P_2O_7$ and $NaPO_3$.

2.2. P_2O_5 -MgO System

The phase diagram of the P_2O_5 -MgO system in the composition ranges from 0 to 50 mol.% P_2O_5 was investigated by Berak [51] using thermal, microscopy and XRD analyses. In this concentration range, three intermediate compounds were observed: $Mg_3P_2O_8$, $Mg_2P_2O_7$ and MgP_2O_6 with melting points at 1630 K, 1655 K and 1438 K, respectively. These phases were considered as line compounds. The temperature of three eutectic reactions $L = MgO + Mg_3P_2O_8$, $L = Mg_3P_2O_8 + \alpha - Mg_2P_2O_7$ and $L = \alpha - Mg_2P_2O_7 + MgP_2O_6$ were found to be 1598 K, 1555 K and 1423 K, respectively. Additionally, $Mg_3P_2O_8$ with two polymorphic forms was confirmed, and its transition temperature was 1328 K. Subsequently, Bobrownicki and Slawski [52] also measured the melting temperature of $Mg_3P_2O_8$ to be 1628 K and the structural transition temperature to be 1323 K. However, these two studies did not give data such as the lattice parameter and the structural transition of $Mg_3P_2O_8$, which have not been reported in subsequent studies [53,54]. Therefore, the optimization process of the present work did not consider the phase transformation of $Mg_3P_2O_8$. Bookey [55], using thermal analysis, investigated the eutectic reaction $L = MgO + Mg_3P_2O_8$ by means of cooling curves, which yielded a reaction temperature of 1603 K. The results were consistent with the data reported by Berak [51]. The melting points of $Mg_3P_2O_8$ and $Mg_2P_2O_7$ were investigated, and the presence of the phase transition in the $Mg_2P_2O_7$ was determined by Czupinska et al. [53] and Oetting et al. [54] using thermal analysis. Combined with the data obtained by Roy et al. [56] and Calvo et al. [57], only the structural transformation of the $Mg_2P_2O_7$ in the low-temperature region was considered in the present work. MgP_4O_{11} was reported to melt congruently at 1183 K by Meyer et al. [32] using DTA. Rakotomahanina-Rolaisoa et al. [58] investigated the melting point of MgP_2O_6 by DTA.

In 1897, Berthelot [59] determined the enthalpy of formation of $Mg_3P_2O_8$ from elements using SCA. In 1952, Bookey et al. [55] investigated the enthalpy of formation of $Mg_3P_2O_8$. In 1954, the enthalpy of formation of $Mg_3P_2O_8$ from elements was measured by Stevens and Turkdogan [60] using SCA. In 1986, Lopatin et al. [61] studied the standard enthalpies of formation of $Mg_2P_2O_7$ and MgP_2O_6 from elements using the Knudsen cell mass spectrometry (KCMS) approach. In 1989, Lopatin et al. [62] used the KCMS method to determine the enthalpy of formation of $Mg_3P_2O_8$ from elements. In 1999, Abdelkader et al. [63] measured the standard enthalpy of formation of $Mg_3P_2O_8$ from elements using the SCA approach. These experimental data on the enthalpies of formation of the compounds in the P_2O_5 -MgO system described above were accepted for the present work. Oetting and McDonald [54] measured the heat capacities of $Mg_3P_2O_8$ and $Mg_2P_2O_7$ using an adiabatic calorimeter and determined the heat contents of $Mg_3P_2O_8$ and $Mg_2P_2O_7$ in the temperature range from 0 to 1700 K. Furthermore, the energy change in the low-temperature phase transition of $Mg_2P_2O_7$ was determined. Iwase et al. [64] investigated the activity of P_2O_5 in liquid P_2O_5 -MgO mixtures using solid oxide galvanic cell techniques at 1673 K. Given that the reported data were obtained from indirect calculations, the data on the activity were not used in the current work.

3. Thermodynamic Modeling

The CALPHAD method is used to formulate a comprehensive thermodynamic model to describe each phase in a system, drawing upon experimental data encompassing phase diagrams, thermodynamic properties and crystal structures. This method rationally selects undetermined parameters to represent each phase of the system as a Gibbs free energy function of variables such as temperature, pressure and composition. Ultimately, the phase diagrams and thermodynamic properties are derived through the utilization of a thermodynamic database containing these Gibbs free energy expressions. In the present study, the thermodynamic assessment of the P_2O_5 - Na_2O and P_2O_5 -MgO systems will be conducted using Thermo-Calc software. Employing the least-squares method, Thermo-Calc software endeavors to align the calculated values with the observed data, seeking optimized variable values that minimize the sum of squared differences between calculated

and experimental data. Hence, the formulation of an appropriate thermodynamic model lays the groundwork for an excellent thermodynamic database.

The following thermodynamic models were used to model the P_2O_5 - Na_2O and P_2O_5 - MgO systems in the present work. The constructed thermodynamic models used for two binary systems are listed in Table 2 and will be described below in more detail.

Table 2. The obtained thermodynamic parameters of the P_2O_5 - Na_2O and P_2O_5 - MgO systems in the present work.

System	Phase	Formula	Thermodynamic Parameter/ $J \cdot mol^{-1}$
P_2O_5 - Na_2O	Liquid	$(Na^{+1})_p(O^{-2}, PO_3^{-1}, PO_4^{-3}, PO_{5/2})_q$	${}^0G_{Na^{+1}:O^{-2}}^{Liquid} = +{}^0G_{Na_2O}^{Liquid}$
			${}^0G_{PO_{5/2}}^{Liquid} = +{}^0G_{P_2O_5}^{Liquid}$
			${}^0G_{Na^{+1}:PO_3^{-1}}^{Liquid} = +0.5{}^0G_{Na_2O}^{Liquid} + 0.5{}^0G_{P_2O_5}^{Liquid} - 223581.5 - 46.8T$
			${}^0G_{Na^{+1}:PO_4^{-3}}^{Liquid} = +1.5{}^0G_{Na_2O}^{Liquid} + 0.5{}^0G_{P_2O_5}^{Liquid} - 597241 + 62T$
			${}^0L_{Na^{+1}:PO_3^{-1},PO_4^{-3}}^{Liquid} = -127756 + 18T$
			${}^1L_{Na^{+1}:PO_3^{-1},PO_4^{-3}}^{Liquid} = -63351$
			${}^0L_{Na^{+1}:O^{-2},PO_4^{-3}}^{Liquid} = +7424$
			${}^0L_{Na^{+1}:PO_3^{-1},PO_{5/2}}^{Liquid} = -48065$
			${}^1L_{Na^{+1}:PO_3^{-1},PO_{5/2}}^{Liquid} = -37884$
			${}^0G_{Na_3PO_4-\alpha}^{Solid} = +{}^0G_{Na_3PO_4}^{Solid}$
	${}^0G_{Na_3PO_4-\beta}^{Solid} = +{}^0G_{Na_3PO_4}^{Solid} + 472 - 0.27T$		
	${}^0G_{Na_4P_2O_7-\alpha}^{Solid} = +{}^0G_{Na_4P_2O_7}^{Solid}$		
	${}^0G_{Na_4P_2O_7-\beta}^{Solid} = +{}^0G_{Na_4P_2O_7}^{Solid} + 10040 - 14.65693431T$		
	${}^0G_{Na_4P_2O_7-\gamma}^{Solid} = +{}^0G_{Na_4P_2O_7}^{Solid} + 13806 - 19.38215388T$		
	${}^0G_{Na_4P_2O_7-\delta}^{Solid} = +{}^0G_{Na_4P_2O_7}^{Solid} + 15061 - 20.94504305T$		
	${}^0G_{Na_4P_2O_7-\epsilon}^{Solid} = +{}^0G_{Na_4P_2O_7}^{Solid} + 17153 - 23.47773070T$		
	${}^0G_{Na_4P_2O_7-\zeta}^{Solid} = +{}^0G_{Na_4P_2O_7}^{Solid} + 20082 - 26.98551513T$		
	${}^0G_{Na_5P_3O_{10}-\alpha}^{Solid} = +{}^0G_{Na_5P_3O_{10}}^{Solid}$		
	${}^0G_{Na_5P_3O_{10}-\beta}^{Solid} = +{}^0G_{Na_5P_3O_{10}}^{Solid} + 10878 - 13.769620T$		
	${}^0G_{NaPO_3-\gamma}^{Solid} = +{}^0G_{NaPO_3}^{Solid}$		
${}^0G_{NaPO_3-\beta}^{Solid} = +{}^0G_{NaPO_3}^{Solid} + 628 - 0.78795483T$			
${}^0G_{NaPO_3-\alpha}^{Solid} = +{}^0G_{NaPO_3}^{Solid} + 4226 - 5.010959525T$			
P_2O_5 - MgO	Liquid	$(Mg^{+2})_p(O^{-2}, PO_3^{-1}, PO_4^{-3}, PO_{5/2})_q$	${}^0G_{Mg^{+2}:O^{-2}}^{Liquid} = +2{}^0G_{MgO}^{Liquid}$
			${}^0G_{PO_{5/2}}^{Liquid} = +{}^0G_{P_2O_5}^{Liquid}$
			${}^0G_{Mg^{+2}:PO_3^{-1}}^{Liquid} = +{}^0G_{MgO}^{Liquid} + {}^0G_{P_2O_5}^{Liquid} - 238484 - 10T$
			${}^0G_{Mg^{+2}:PO_4^{-3}}^{Liquid} = +3{}^0G_{MgO}^{Liquid} + {}^0G_{P_2O_5}^{Liquid} - 709347 + 185T$
			${}^0L_{Mg^{+2}:PO_3^{-1},PO_4^{-3}}^{Liquid} = -128900 + 45T$
			${}^1L_{Mg^{+2}:PO_3^{-1},PO_4^{-3}}^{Liquid} = +13365$
			${}^2L_{Mg^{+2}:PO_3^{-1},PO_4^{-3}}^{Liquid} = -16547$
			${}^3L_{Mg^{+2}:PO_3^{-1},PO_4^{-3}}^{Liquid} = +40441$
			${}^0L_{Mg^{+2}:O^{-2},PO_4^{-3}}^{Liquid} = -57701$

Table 2. Cont.

System	Phase	Formula	Thermodynamic Parameter/J·mol ⁻¹
			${}^1L_{Mg^{+2}:O^{-2},PO_4^{-3}} = +6541$
			${}^2L_{Mg^{+2}:O^{-2},PO_4^{-3}} = -8954$
			${}^0L_{Mg^{+2}:PO_3^{-1},PO_{5/2}} = -92054 + 60T$
			${}^1L_{Mg^{+2}:PO_3^{-1},PO_{5/2}} = -25546$
			${}^2L_{Mg^{+2}:PO_3^{-1},PO_{5/2}} = -35451$
			${}^0L_{Mg^{+2}:O^{-2},PO_3^{-1}} = -66748 + 51T$
	Mg ₃ P ₂ O ₈	(Mg ⁺²) ₃ (P ⁺⁵) ₂ (O ⁻²) ₈	${}^0G_{Mg_3P_2O_8}^{Mg^{+2},P^{+5},O^{-2}} = +{}^0G_{Mg_3P_2O_8}^{Solid}$
	Mg ₂ P ₂ O _{7-β}	(Mg ⁺²) ₂ (P ⁺⁵) ₂ (O ⁻²) ₇	${}^0G_{Mg_2P_2O_{7-\beta}}^{Mg^{+2},P^{+5},O^{-2}} = +{}^0G_{Mg_2P_2O_7}^{Solid}$
	Mg ₂ P ₂ O _{7-α}	(Mg ⁺²) ₂ (P ⁺⁵) ₂ (O ⁻²) ₇	${}^0G_{Mg_2P_2O_{7-\alpha}}^{Mg^{+2},P^{+5},O^{-2}} = +{}^0G_{Mg_2P_2O_7}^{Solid} + 680 - 2.0T$
	MgP ₂ O ₆	(Mg ⁺²) ₁ (P ⁺⁵) ₂ (O ⁻²) ₆	${}^0G_{MgP_2O_6}^{Mg^{+2},P^{+5},O^{-2}} = +{}^0G_{MgP_2O_6}^{Solid}$
	MgP ₄ O ₁₁	(Mg ⁺²) ₁ (P ⁺⁵) ₄ (O ⁻²) ₁₁	${}^0G_{MgP_4O_{11}}^{Mg^{+2},P^{+5},O^{-2}} = +{}^0G_{MgP_4O_{11}}^{Solid}$
Function	Temperature range/K		
${}^0G_{P_2O_5}^{Liquid}$	(298.15–1000)		$-1639225.067 - 230.7480381T + 21.643407T \ln T - 0.1681142T^2 + 1.87715 \times 10^{-5}T^3 + 1758186.5T^{-1} + 22900.402 \ln T$
	(1000–6000)		$-1579441.75 + 1382.959261T - 225T \ln T$
${}^0G_{P_2O_5}^{P_2O_5-OO}$	(298.15–1000)		$-1665880.067 - 199.4980381T + 21.643407T \ln T - 0.1681142T^2 + 1.87715 \times 10^{-5}T^3 + 1758186.5T^{-1} + 22900.402 \ln T$
	(1000–6000)		$-1606096.75 + 1414.209261T - 225T \ln T$
${}^0G_{P_2O_5}^{P_2O_5-O}$	(298.15–1000)		$-1666269.067 - 198.3480381T + 21.643407T \ln T - 0.1681142T^2 + 1.87715 \times 10^{-5}T^3 + 1758186.5T^{-1} + 22900.402 \ln T$
	(1000–6000)		$-1606485.75 + 1415.359261T - 225T \ln T$
${}^0G_{P_2O_5}^{P_2O_5-H}$	(298.15–1000)		$-1631835.067 - 221.1390381T + 21.643407T \ln T - 0.1681142T^2 + 1.87715 \times 10^{-5}T^3 + 1758186.5T^{-1} + 22900.402 \ln T$
	(1000–6000)		$-1572051.75 + 1392.568261T - 225T \ln T$
${}^0G_{Na_2O}^{Liquid}$	(298.15–1405)		$-380898.2803 + 340.194781T - 66.216001T \ln T - 0.021932551T^2 + 2.34792 \times 10^{-6}T^3 + 406685.01T^{-1}$
	(1405–1500)		$-387789.21 + 580.2481164T - 104.6T \ln T$
${}^0G_{Na_2O}^{Na_2O-\alpha}$	(298.15–1405)		$-428595.8803 + 374.143281T - 66.216001T \ln T - 0.021932551T^2 + 2.34792 \times 10^{-6}T^3 + 406685.01T^{-1}$
	(1405–1500)		$-435486.81 + 614.1966164T - 104.6T \ln T$
${}^0G_{Na_2O}^{Na_2O-\beta}$	(298.15–1405)		$-440520.2803 + 383.736481T - 66.216001T \ln T - 0.021932551T^2 + 2.34792 \times 10^{-6}T^3 + 406685.01T^{-1}$
	(1405–1500)		$-447411.21 + 623.7898164T - 104.6T \ln T$
${}^0G_{Na_2O}^{Na_2O-\gamma}$	(298.15–1405)		$-442277.5603 + 385.454281T - 66.216001T \ln T - 0.021932551T^2 + 2.34792 \times 10^{-6}T^3 + 406685.01T^{-1}$
	(1405–1500)		$-449168.49 + 625.5076164T - 104.6T \ln T$
${}^0G_{Na_3PO_4}^{Solid}$	(298.15–6000)		$+{}^0G_{Na_2O}^{Na_2O-\gamma} + 0.5{}^0G_{P_2O_5}^{P_2O_5-H} - 520688.946 - 4.353T$
${}^0G_{Na_4P_2O_7}^{Solid}$	(298.15–967)		$-3282062.70195 + 815.816308T - 145.08494T \ln T - 0.215875T^2 + 3.77148 \times 10^{-5}T^3 + 542554.7741T^{-1}$
	(967–1273)		$-3322276.2378 + 2062.32142T - 349.82659T \ln T$
${}^0G_{Na_5P_3O_{10}}^{Solid}$	(298.15–6000)		$+2.5{}^0G_{Na_2O}^{Na_2O-\gamma} + 1.5{}^0G_{P_2O_5}^{P_2O_5-H} - 1144087.404 - 20.487T$
${}^0G_{NaPO_3}^{Solid}$	(298.15–703)		$-1243133.8886 + 264.3713457T - 46.08288T \ln T - 0.09082T^2 + 1.80447 \times 10^{-5}T^3 + 188542.1015T^{-1}$
	(703–973)		$-1256643.34549 + 704.6628499T - 119.50568T \ln T$
${}^0G_{MgO}^{Liquid}$	(298.15–1700)		$-549098.33 + 275.724634T - 47.4817T \ln T - 0.00232681T^2 + 4.5043 \times 10^{-8}T^3 + 516900T^{-1}$
	(1700–2450)		$-585159.646 + 506.06825T - 78.3772T \ln T + 0.0097344T^2 - 8.60338 \times 10^{-7}T^3 + 8591550T^{-1}$

Table 2. Cont.

System	Phase	Formula	Thermodynamic Parameter/J·mol ⁻¹
${}^0G_{MgO}^{Solid}$		(2450–3100)	$+9110429.75 - 42013.7634T + 5298.548T\ln T - 1.30122485T^2 + 5.8262601 \times 10^{-5}T^3 - 3.24037416 \times 10^9T^{-1}$
		(3100–5100)	$-632664.468 + 589.239555T - 84T\ln T$
		(298.15–1700)	$-619428.502 + 298.253571T - 47.4817T\ln T - 0.00232681T^2 + 4.5043 \times 10^{-8}T^3 + 516900T^{-1}$
		(1700–3100)	$-655489.818 + 528.597187T - 78.3772T\ln T + 0.0097344T^2 - 8.60338 \times 10^{-7}T^3 + 8591550T^{-1}$
		(3100–5000)	$-171490.159 - 1409.43369T + 163.674142T\ln T - 0.044009535T^2 + 1.374896 \times 10^{-6}T^3 - 1.72665403 \times 10^8T^{-1}$
		(5000–5100)	$-722412.718 + 617.657452T - 84T\ln T$
${}^0G_{Mg_3P_2O_8}^{Solid}$		(298.15–1800)	$-3863914.664 + 1191.277265T - 195.04422T\ln T - 0.098665T^2 + 9.22527 \times 10^{-6}T^3 + 1562390.321T^{-1}$
${}^0G_{Mg_2P_2O_7}^{Solid}$		(298.15–1800)	$-3217696.802 + 1003.594497T - 165.99611T\ln T - 0.07885T^2 + 7.96388 \times 10^{-6}T^3 + 1371185.587T^{-1}$
${}^0G_{MgP_2O_6}^{Solid}$		(298.15–6000)	$+{}^0G_{MgO}^{Solid} + {}^0G_{P_2O_5}^{P_2O_5-H} - 240840 + 2.95T$
${}^0G_{MgP_4O_{11}}^{Solid}$		(298.15–6000)	$+{}^0G_{MgO}^{Solid} + {}^0G_{P_2O_5}^{P_2O_5-H} - 269030 - 4.29T$

3.1. Pure Unary Component

The Gibbs energy $G_i(T)$ of pure unary component i can be expressed as follows:

$$G_i(T) - H_i^{SER} = a + bT + cT\ln T + dT^2 + eT^{-2} + fT^3 + gT^7 + hT^{-9} \quad (1)$$

where H_i^{SER} is the standard molar enthalpy of pure unary component i at 298.15 K and 101,325 Pa, J·mol⁻¹; $a-h$ are the parameters to be optimized; T is the thermodynamic temperature, K.

3.2. Liquid Phase

In the current assessment, the ionic two-sublattice model is used to describe the liquid phase of the P₂O₅-Na₂O and P₂O₅-MgO systems. The ionic two-sublattice model assumes that cations only mix with each other, and anions only mix with each other. This model comprises two sublattices: one for cations and the other for anions, neutrals, and vacancies.

In the liquid phase of the P₂O₅-Na₂O and P₂O₅-MgO systems, the content of anions such as PO₃⁻¹, P₂O₇⁻⁴, PO₄⁻³ varies with the composition of the system oxides [8]. To simplify the thermodynamic model by reducing the thermodynamic parameters, only the two anions (PO₃⁻¹ and PO₄⁻³) are considered in the optimized modeling process. Therefore, the thermodynamic models of the liquid phase of the P₂O₅-Na₂O and P₂O₅-MgO systems are (Na⁺¹)_P(O⁻², PO₃⁻¹, PO₄⁻³, PO_{5/2})_Q and (Mg⁺²)_P(O⁻², PO₃⁻¹, PO₄⁻³, PO_{5/2})_Q, where P and Q denote the total valence of the anion sublattice and the total valence of the cation sublattice, respectively. To maintain the electroneutrality of the liquid phase of the systems, the stoichiometric factors P and Q are allowed to change with the composition of the system oxides. Taking the P₂O₅-Na₂O system as an example, the Gibbs energy of the liquid phase is expressed as follows:

$$G_m^{Liquid} - H_i^{SER} = y_{Na^{+1}}y_{O^{-2}}G_{Na^{+1}:O^{-2}}^{Liquid} + y_{Na^{+1}}y_{PO_3^{-1}}G_{Na^{+1}:PO_3^{-1}}^{Liquid} + y_{Na^{+1}}y_{PO_4^{-3}}G_{Na^{+1}:PO_4^{-3}}^{Liquid} + Q(y_{PO_{5/2}}\ln y_{PO_{5/2}}) + PRT(y_{Na^{+1}}\ln y_{Na^{+1}}) + QRT(y_{O^{-2}}\ln y_{O^{-2}} + y_{PO_3^{-1}}\ln y_{PO_3^{-1}} + y_{PO_4^{-3}}\ln y_{PO_4^{-3}} + y_{PO_{5/2}}\ln y_{PO_{5/2}}) + {}^E G_m^{Liquid} \quad (2)$$

where H_i^{SER} is the molar enthalpy of the pure unary component in the reference state of the standard element at 298.15 K and 101,325 Pa, J·mol⁻¹; y is the site fraction of each species in the liquid phase in their respective sublattices; G is the Gibbs energy for the formation of the end-member, J·mol⁻¹; R is the gas constant ($R = 8.314 \text{ J} \cdot (\text{mol} \cdot \text{K})^{-1}$); ${}^E G_m^{Liquid}$ is the excess Gibbs energy, J·mol⁻¹, which is denoted as follows:

$$\begin{aligned}
E G_m^{Liquid} = & y_{Na^{+1}} y_{O^{-2}} y_{PO_3^{-1}} {}^0 L_{Na^{+1}:O^{-2},PO_3^{-1}}^{Liquid} + y_{Na^{+1}} y_{O^{-2}} y_{PO_4^{-3}} ({}^0 L_{Na^{+1}:O^{-2},PO_4^{-3}}^{Liquid} + {}^1 L_{Na^{+1}:O^{-2},PO_4^{-3}}^{Liquid} (y_{O^{-2}} - y_{PO_4^{-3}}) \\
& + {}^2 L_{Na^{+1}:O^{-2},PO_4^{-3}}^{Liquid} (y_{O^{-2}} - y_{PO_4^{-3}})^2) + y_{Na^{+1}} y_{O^{-2}} y_{PO_5/2} {}^0 L_{Na^{+1}:O^{-2},PO_5/2}^{Liquid} \\
& + y_{Na^{+1}} y_{PO_3^{-1}} y_{PO_4^{-3}} ({}^0 L_{Na^{+1}:PO_3^{-1},PO_4^{-3}}^{Liquid} + {}^1 L_{Na^{+1}:PO_3^{-1},PO_4^{-3}}^{Liquid} (y_{PO_3^{-1}} - y_{PO_4^{-3}}) \\
& + {}^2 L_{Na^{+1}:PO_3^{-1},PO_4^{-3}}^{Liquid} (y_{PO_3^{-1}} - y_{PO_4^{-3}})^2 + {}^3 L_{Na^{+1}:PO_3^{-1},PO_4^{-3}}^{Liquid} (y_{PO_3^{-1}} - y_{PO_4^{-3}})^3) \\
& + y_{Na^{+1}} y_{PO_3^{-1}} y_{PO_5/2} ({}^0 L_{Na^{+1}:PO_3^{-1},PO_5/2}^{Liquid} + {}^1 L_{Na^{+1}:PO_3^{-1},PO_5/2}^{Liquid} (y_{PO_3^{-1}} - y_{PO_5/2}) \\
& + {}^2 L_{Na^{+1}:PO_3^{-1},PO_5/2}^{Liquid} (y_{PO_3^{-1}} - y_{PO_5/2})^2) + y_{Na^{+1}} y_{PO_4^{-3}} y_{PO_5/2} {}^0 L_{Na^{+1}:PO_4^{-3},PO_5/2}^{Liquid}
\end{aligned} \tag{3}$$

where ${}^i L^{Liquid}$ ($i = 0, 1, 2, 3$) represents the interaction of the species in each sublattice and is the interaction parameter to be optimized.

3.3. Intermediate Compounds

In this work, all solid phases Na_3PO_4 , $Na_4P_2O_7$, $Mg_3P_2O_8$, $Mg_2P_2O_7$, etc., are described as stoichiometric compounds. For the solid phase with heat capacity data, the Gibbs free energy G_m is expressed as follows:

$$G_m - H^{SER} = a + bT + cT \ln T + dT^2 + eT^{-1} \tag{4}$$

where H^{SER} is the molar enthalpy of the pure elements (Na, Mg, P and O) in the reference state of the standard element at 298.15 K and 101,325 Pa, $J \cdot mol^{-1}$; $a \sim e$ are the parameters which will be optimized; T is the thermodynamic temperature, K.

For the solid phase lacking heat capacity data, taking the P_2O_5 - Na_2O system as an example, the Gibbs energy ${}^0 G_m$ of the solid is expressed as follows:

$${}^0 G_m - H^{SER} = x {}^0 G_{Na_2O}^{Na_2O-\gamma} + y {}^0 G_{P_2O_5}^{P_2O_5-H} + A + BT \tag{5}$$

where x and y are the ratios of Na_2O and P_2O_5 in the solid phase; ${}^0 G_{Na_2O}^{Na_2O-\gamma}$ and ${}^0 G_{P_2O_5}^{P_2O_5-H}$ are the Gibbs energy of the solid phase of Na_2O and P_2O_5 , respectively, $J \cdot mol^{-1}$; A and B are the parameters which will be evaluated.

4. Results and Discussion

The thermodynamic optimization of the P_2O_5 - Na_2O and P_2O_5 - MgO binary systems was carried out based on the critical evaluation of phase equilibrium and thermodynamic property data using Thermo-Calc software in the current study. During the optimization process, certain emphasis was given to each dataset of phase equilibrium and thermodynamic property data, taking into account their reliability. By adjusting the thermodynamic parameters for each phase within the systems, the calculated results could reasonably describe the experimental data within the acceptable error range.

Initially, the solid-phase parameters were optimized using experimental data, encompassing the heat capacity and formation enthalpy of the intermediate phases. Subsequently, liquid-phase parameters were incorporated to replicate the liquidus and invariant reactions of the systems. Finally, all parameters were simultaneously optimized by considering all reliable experimental data to obtain a set of thermodynamic parameters capable of effectively describing the P_2O_5 - Na_2O and P_2O_5 - MgO binary systems, as presented in Table 2.

4.1. P_2O_5 - Na_2O System

The Gibbs energy functions for the components P_2O_5 and Na_2O were sourced from the works of Jung et al. [65] and Wu et al. [66], respectively. Initially, the heat capacities of polymorphic forms of $Na_4P_2O_7$ and $NaPO_3$ were determined by fitting experimental

data from Andon et al. [47], Ashcroft et al. [48] and Lazarev et al. [49], which were treated as identical within this study. Subsequently, the formation enthalpies of the four intermediate phases were optimized using experimental data on formation enthalpies from elements [40–46]. Then, the liquid parameters such as ${}^0L_{Na^{+1}:PO_3^{-1},PO_4^{-3}}$, ${}^1L_{Na^{+1}:PO_3^{-1},PO_4^{-3}}$, etc., were adjusted to replicate the liquidus and invariant reactions of the P_2O_5 - Na_2O binary system. Finally, all parameters were optimized simultaneously by considering all available experimental data.

Figure 1 presents the optimized phase diagram of the P_2O_5 - Na_2O binary system in comparison with experimental data [34–39]. The eutectic reactions $L = \beta - NaPO_3 + \alpha - Na_5P_3O_{10}$ and $L = \alpha - Na_4P_2O_7 + \beta - Na_3PO_4$ are calculated to occur at temperatures of 820 K and 1212 K, respectively, while the peritectic reaction $L + \alpha - Na_4P_2O_7 = \alpha - Na_5P_3O_{10}$ takes place at 895 K. The difference in the calculated $X(Na_2O)$ from the experimentally determined values reported in the literature is less than 0.9 mol.%, marking a substantial improvement over the calculation of Xie et al. [7] and aligning more closely with the experimental data. Due to the limited availability of liquidus data for the P_2O_5 - Na_2O system, the predicted temperatures for the $L = \gamma - NaPO_3 + O' - P_2O_5$ and $L = \beta - Na_3PO_4 + \beta - Na_2O$ reactions calculated in this study are 560 K and 1220 K, respectively, which warrant validation through further experiments. The calculated liquidus points generally correspond well with the experimental data in the literature. Table 3 provides a comparison of the calculated invariant reactions involving the liquid phase in the P_2O_5 - Na_2O binary system with experimental data. It is evident that the calculated results of this study can effectively describe most of the available experimental information.

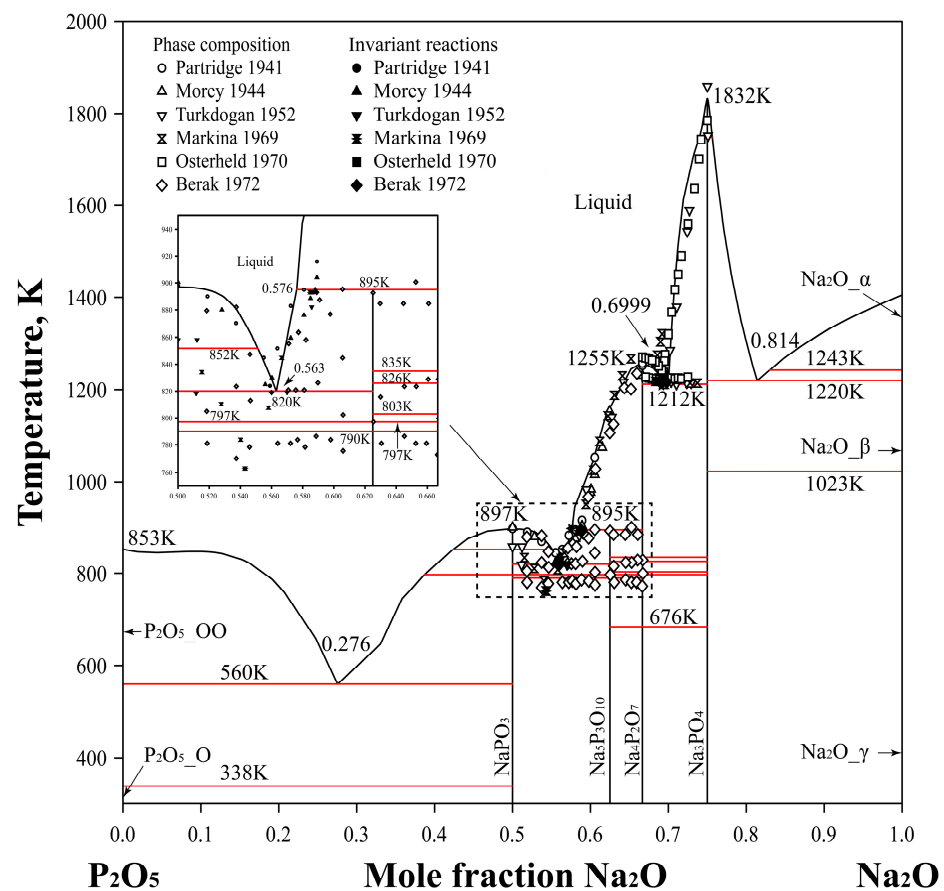
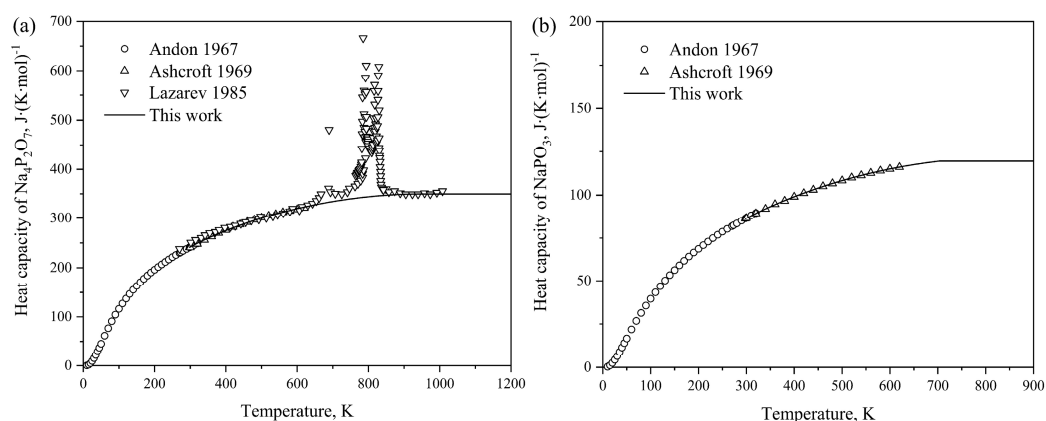


Figure 1. Calculated phase diagram of the P_2O_5 - Na_2O binary system compared with the experimental data [34–39].

Table 3. Calculated invariant reactions involving the liquid phase in the P_2O_5 - Na_2O binary system.

Reaction	Type	Liquid Composition/Mole Fraction Na_2O	Temperature/K	Reference
$L = \gamma - NaPO_3 + O' - P_2O_5$	Eutectic	0.276	560	This work
$L = \beta - NaPO_3 + \alpha - Na_5P_3O_{10}$	Eutectic	0.559	824	[34]
		0.556	825	[35]
		0.57	819	[36]
		0.543	763	[37]
		0.56	819	[39]
		0.56	833	[7]
		0.563	820	This work
$L + \alpha - Na_4P_2O_7 = \alpha - Na_5P_3O_{10}$	Peritectic	0.587	893	[34]
		0.588	895	[35]
		0.585	893	[37]
		0.589	893	[39]
		0.575	898	[7]
		0.576	895	This work
$L = \alpha - Na_4P_2O_7 + \beta - Na_3PO_4$	Eutectic	0.684	1218	[37]
		0.694	1225	[38]
		0.6975	1217	[39]
		0.691	1209	[7]
		0.6999	1212	This work
$L = \beta - Na_3PO_4 + \beta - Na_2O$	Eutectic	0.814	1220	This work

Utilizing the optimized thermodynamic parameters, the thermodynamic properties of the P_2O_5 - Na_2O system are computed. Figure 2a and b show the calculated heat capacities of $Na_4P_2O_7$ and $NaPO_3$, respectively, obtained in this study, juxtaposed with experimental data measured by Andon et al. [47], Ashcroft et al. [48] and Lazarev et al. [49]. The calculated results exhibit satisfactory agreement with the measured values. For $Na_5P_3O_{10}$ and Na_3PO_4 , the Neumann–Kopp equation was employed to describe their heat capacities due to the limited experimental data available. The standard enthalpies of formation of the intermediate compounds from elements (BCC_A2 for sodium and white phosphorus) at 298 K are also calculated in this work, as depicted in Figure 3. The graph illustrates that our calculated results are generally consistent with the experimental values from Refs. [40–46]. Considering experimental uncertainties, the calculations are deemed acceptable.

**Figure 2.** Calculated heat capacities of $Na_4P_2O_7$ (a) and $NaPO_3$ (b) compared with the experimental data [47–49].

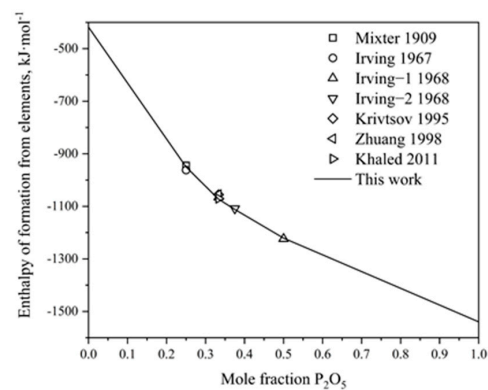


Figure 3. Calculated enthalpies of formation for the intermediate compounds of the P_2O_5 - Na_2O binary system at 298.15 K from elements compared with the experimental data [40–46].

4.2. P_2O_5 - MgO System

The Gibbs energy functions for the components P_2O_5 and MgO utilized in this study were sourced from Jung et al. [65] and Mao et al. [67], respectively. The heat capacities of $Na_4P_2O_7$ and $NaPO_3$ were modeled using experimental data from Oetting et al. [54]. In the present research, it is assumed that the heat capacities of both allotropic forms of $Mg_2P_2O_7$ were equal. The optimized phase diagram of the P_2O_5 - MgO system, presented in Figure 4, is compared with experimental data [32,51,53–58]. Additionally, the temperature and phase composition details of invariant reactions are juxtaposed with the experimental data reported in the literature, as shown in Table 4. It is evident that the calculated phase boundaries align well with the experimental information found in the literature. The present study provides a better and more reasonable description of the experimental data for the P_2O_5 - MgO system compared to the results of Ding et al. [8].

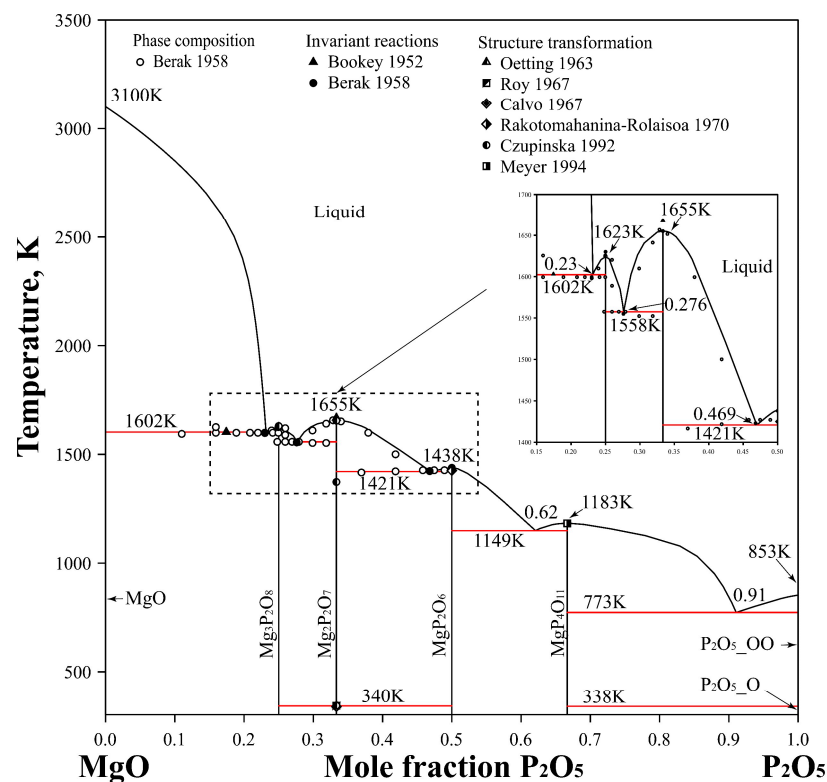


Figure 4. Calculated phase diagram of the P_2O_5 - MgO binary system compared with the experimental data [32,51,53–58].

Table 4. Calculated invariant reactions involving the liquid phase in the P₂O₅-MgO binary system.

Reaction	Type	Liquid Composition/Mole Fraction P ₂ O ₅	Temperature/K	Reference
L = MgO + Mg ₃ P ₂ O ₈	Eutectic	0.23	1598	[51]
		-	1603	[55]
		0.23	1596	[8]
		0.23	1602	This work
		0.276	1555	[51]
L = Mg ₃ P ₂ O ₈ + α - Mg ₂ P ₂ O ₇	Eutectic	0.277	1563	[8]
		0.276	1558	This work
		0.468	1423	[51]
L = α - Mg ₂ P ₂ O ₇ + MgP ₂ O ₆	Eutectic	0.469	1410	[8]
		0.469	1421	This work
		0.62	1149	This work
L = MgP ₂ O ₆ + MgP ₄ O ₁₁	Eutectic	0.91	773	This work
L = MgP ₄ O ₁₁ + O' - P ₂ O ₅	Eutectic			

The phase relationship in the composition range above 50 mol.% P₂O₅ remains to be definitively determined experimentally, owing to the limited available experimental data. In the optimization process, two eutectic reactions were predicted in this portion of the phase diagram. The calculated reaction temperatures are 1149 K for the reaction L = MgP₂O₆ + MgP₄O₁₁ and 773 K for the reaction L = MgP₄O₁₁ + O' - P₂O₅. Correspondingly, the calculated X(P₂O₅) values are 62 mol.% and 91 mol.%, respectively.

The heat capacities of Mg₃P₂O₈ and Mg₂P₂O₇ obtained by optimization in this work are illustrated in Figure 5a,b. Reasonable agreement is obtained between our calculated results and the heat capacities of Mg₃P₂O₈ and Mg₂P₂O₇ in the temperature range from 298.15 K to 1800 K determined by Oetting et al. [54]. To describe the heat capacities of MgP₂O₆ and MgP₄O₁₁, the Neumann–Kopp equation was employed during the optimization process to sum the heat capacities of Na2O_γ and P2O5_H. Figure 6a,b present the calculated heat contents of Mg₃P₂O₈ and Mg₂P₂O₇ based on the obtained thermodynamic parameters, compared with the experimental data [54]. The results indicate a close alignment with the experimental values, with acceptable deviations considering experimental errors. The calculated melting enthalpy of Mg₃P₂O₈ ($\Delta H_{melt} = 97.449 \text{ kJ}\cdot\text{mol}^{-1}$) is slightly lower than the experimental value reported by Oetting et al. [54], while the calculated melting enthalpy of Mg₂P₂O₇ ($\Delta H_{melt} = 160.03 \text{ kJ}\cdot\text{mol}^{-1}$) is slightly higher than the experimental value. This brings the calculated values much closer to the experimental results compared to the study by Ding et al. [8]. Additionally, the calculated enthalpy of transition from Mg₂P₂O_{7_β} to Mg₂P₂O_{7_α} at 340 K is determined to be 0.68 kJ·mol⁻¹. Figure 7 shows the calculated standard enthalpies of formation for the intermediate compounds from elements at 298 K compared with the experimental data [55,59–63] and calculated results from the literature [8]; the reference states are the Mg of HCP_A3 and white phosphorus, which reproduce the standard enthalpy of formation for the compounds from elements very well. As can be seen, a precise description of the experimental thermodynamic properties of the system can be provided by utilizing the calculated thermodynamic parameters within the acceptable margin of error.

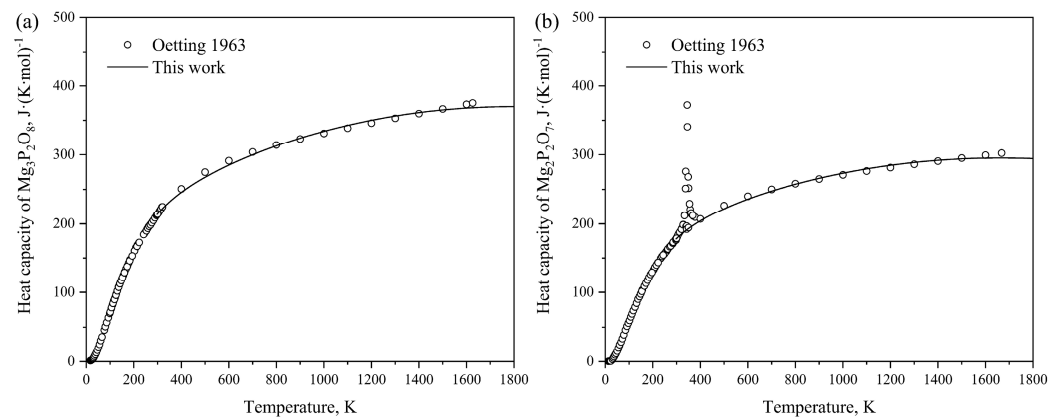


Figure 5. Calculated heat capacities of $\text{Mg}_3\text{P}_2\text{O}_8$ (a) and $\text{Mg}_2\text{P}_2\text{O}_7$ (b) compared with the experimental data [54].

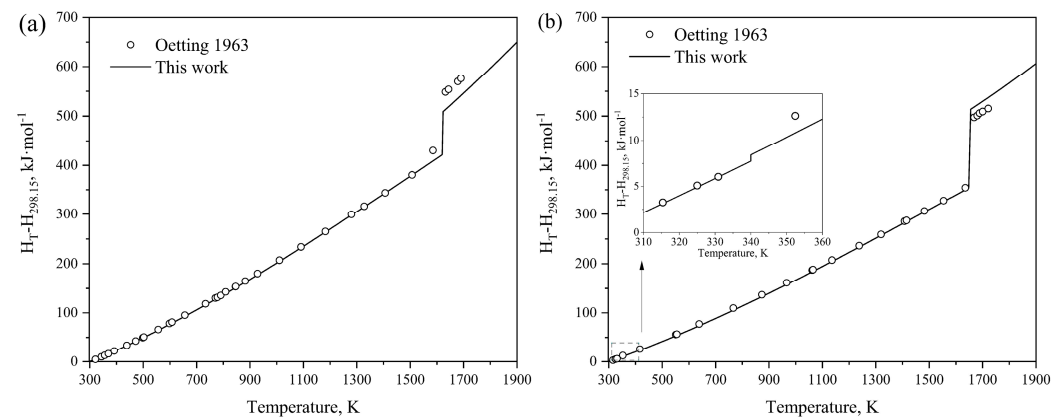


Figure 6. Calculated heat contents of $\text{Mg}_3\text{P}_2\text{O}_8$ (a) and $\text{Mg}_2\text{P}_2\text{O}_7$ (b) compared with the experimental data [54].

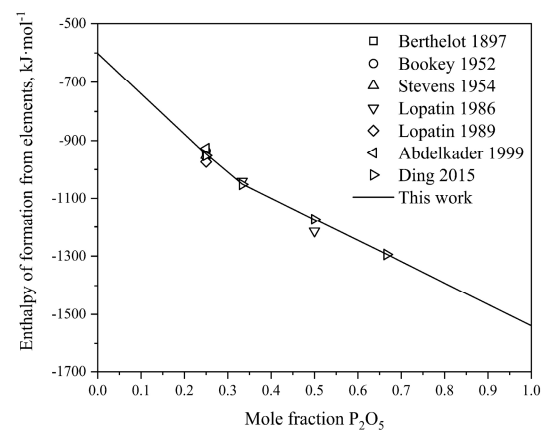


Figure 7. Calculated enthalpies of formation for the intermediate compounds of the P_2O_5 - MgO binary system at 298.15 K from elements compared with the experimental data [55,59–63] and calculated results from the literature [8].

5. Conclusions

The CALPHAD method was utilized to critically evaluate and assess the P_2O_5 - Na_2O and P_2O_5 - MgO binary systems. The main conclusions are summarized below:

1. A set of self-consistent thermodynamic parameters is derived for the P_2O_5 - Na_2O and P_2O_5 - MgO binary systems based on a critical evaluation of the available phase diagram and thermodynamic property data. The calculated phase diagrams and

- thermodynamic properties employing the obtained thermodynamic parameters well reproduce the data reported in the literature.
2. In comparison with the previous assessments using the modified quasi-chemical model for the liquid phase, the present study using the ionic two-sublattice model to express the liquid phase for the first time can describe the experimental data of the P_2O_5 - Na_2O and P_2O_5 - MgO binary systems in a better and more reasonable way, particularly the invariant reactions involving the liquid phase. The difference in the phase composition and temperature of invariant reactions from the experimentally determined values reported in the literature is less than 0.9 mol.% and 5K, respectively.
 3. Four eutectic reactions ($L = \gamma - NaPO_3 + O' - P_2O_5$, $L = \beta - Na_3PO_4 + \beta - Na_2O$, $L = MgP_2O_6 + MgP_4O_{11}$ and $L = MgP_4O_{11} + O' - P_2O_5$) are predicted in the P_2O_5 - Na_2O and P_2O_5 - MgO binary systems. The predicted temperatures of these eutectic reactions are 560 K, 1220 K, 1149 K and 773 K, with the corresponding phase compositions $X(P_2O_5)$ being 82.4 mol%, 18.6 mol%, 62 mol% and 91 mol%, respectively. These predictions await further experimental validation.

Author Contributions: Conceptualization, L.Z. and L.Y.; methodology, L.Y.; software, C.L.; validation, J.Y.; formal analysis, L.Y. and G.X.; investigation, L.Y. and Z.D.; resources, L.Y. and C.L.; data curation, L.Y.; writing—original draft preparation, L.Y.; writing—review and editing, L.Y. and Y.J.; visualization, L.L.; supervision, L.Z. and Y.J.; project administration, L.Z.; funding acquisition, L.Z. and Y.J. All authors have read and agreed to the published version of the manuscript.

Funding: This research was funded by the Hunan Provincial Natural Science Foundation of China (No. 2022JJ80069) and supported by the National Key Research and Development Program of China (No. 2022YFC3900902).

Institutional Review Board Statement: Not applicable.

Informed Consent Statement: Not applicable.

Data Availability Statement: The original contributions presented in the study are included in the article, further inquiries can be directed to the corresponding authors.

Conflicts of Interest: The authors declare that they have no conflicts of interest.

References

1. Suito, H.; Inoue, R. Effects of Na_2O and BaO additions on phosphorus distribution between CaO - MgO - FeO - SiO_2 -slags and liquid iron. *Trans. Iron Steel Inst. Jpn.* **1984**, *24*, 47–53. [\[CrossRef\]](#)
2. Chen, T.; Yuan, Y.; Wang, J.; Wu, J.; Wang, B.; Chen, X.; Moelans, N.; Wang, J.; Pan, F. Features and classification of solid solution behavior of ternary Mg alloys. *J. Magnes. Alloys* **2024**. [\[CrossRef\]](#)
3. Chen, T.; Gao, Q.; Yuan, Y.; Li, T.; Xi, Q.; Liu, T.; Tang, A.; Watson, A.; Pan, F. Coupling physics in machine learning to investigate the solution behavior of binary Mg alloys. *J. Magnes. Alloys* **2021**, *10*, 2817–2832. [\[CrossRef\]](#)
4. Yi, W.; Liu, G.; Gao, J.; Zhang, L. Boosting for concept design of casting aluminum alloys driven by combining computational thermodynamics and machine learning techniques. *J. Mater. Inf.* **2021**, *1*, 11. [\[CrossRef\]](#)
5. Zhang, S.; Yi, W.; Zhong, J.; Gao, J.; Lu, Z.; Zhang, L. Computer alloy design of Ti modified Al-Si-Mg-Sr casting alloys for achieving simultaneous enhancement in strength and ductility. *Materials* **2022**, *16*, 306. [\[CrossRef\]](#) [\[PubMed\]](#)
6. Tian, Y.; Jiang, K.; Deng, Z.; Wang, K.; Zhang, H.; Liu, L.; Zhang, L. Integration of CALPHAD calculations and nanoindentation test for the design of low-modulus near- β titanium. *J. Cent. South Univ.* **2023**, *30*, 3940–3949. [\[CrossRef\]](#)
7. Xie, W.; Wei, S.H.; Hudon, P.; Jung, I.; Qiao, Z.; Cao, Z. Critical evaluation and thermodynamic assessment of the R_2O - P_2O_5 ($R = Li, Na$ and K) systems. *Calphad* **2020**, *68*, 101718. [\[CrossRef\]](#)
8. Ding, G.; Xie, W.; Jung, I.; Qiao, Z.; Du, G.; Cao, Z. Thermodynamic assessment of the MgO - P_2O_5 and CaO - P_2O_5 Systems. *Acta Phys.-Chim. Sin.* **2015**, *31*, 1853–1863. [\[CrossRef\]](#)
9. Zhang, L.; Gao, F.; Deng, T.; Liu, Y.; Yang, L.; Guo, C.; Tan, J.; Ma, T.; Chen, W.; Du, Y. Phase equilibria in the FeO - Fe_2O_3 - SiO_2 system: Experimental measurement and thermodynamic modeling. *Calphad* **2022**, *79*, 102459. [\[CrossRef\]](#)
10. Yang, L.; Zeng, Y.; Guo, C.; Liu, Y.; Li, B.; Deng, T.; Chen, W.; Du, Y. Experimental investigation and thermodynamic assessment of the Na_2O - Al_2O_3 - CaO system. *Ceram. Int.* **2024**, *50*, 13422. [\[CrossRef\]](#)
11. Zhang, L.; Liu, Y.; Gao, F.; Tan, J.; Yang, L.; Deng, T.; Chen, W.; Ouyang, Y.; Du, Y. Thermodynamic description of the FeO - Fe_2O_3 - MgO system and its extrapolation to the X - MgO - FeO - Fe_2O_3 ($X = CaO$ and SiO_2) systems. *J. Am. Ceram. Soc.* **2024**, *107*, 4358–4372. [\[CrossRef\]](#)

12. Wiench, D.M.; Jansen, M. Untersuchungen an Tetranatrium-cyclo-tetraphosphat(V) und seinen Hydraten. *Monatsh. Chem.* **1983**, *114*, 699–709. [[CrossRef](#)]
13. Ondik, H.M. The structure of anhydrous sodium trimetaphosphate $\text{Na}_3\text{P}_3\text{O}_9$, and the monohydrate, $\text{Na}_3\text{P}_3\text{O}_9 \cdot \text{H}_2\text{O}$. *Acta Crystallogr.* **1965**, *18*, 226–232. [[CrossRef](#)]
14. Jost, K.H. Die Struktur des Kurrol'schen Na-Salzes $(\text{NaPO}_3)_x$, Typ B. *Acta Crystallogr.* **1963**, *16*, 640–642. [[CrossRef](#)]
15. Corbridge, D.E.C. Crystallographic data on some Kurrol salts. *Acta Crystallogr.* **1955**, *8*, 520. [[CrossRef](#)]
16. Dymon, J.J.; King, A.J. Structure studies of the two forms of sodium tripolyphosphate. *Acta Crystallogr.* **1951**, *4*, 378–379. [[CrossRef](#)]
17. Corbridge, D.E.C. The crystal structure of sodium triphosphate, $\text{Na}_5\text{P}_3\text{O}_{10}$, phase I. *Acta Crystallogr.* **1960**, *13*, 263–269. [[CrossRef](#)]
18. Leung, K.Y.; Calvo, C. The Structure of $\text{Na}_4\text{P}_2\text{O}_7$ at 22 °C. *Can. J. Chem.* **1972**, *50*, 2519–2526. [[CrossRef](#)]
19. Lissel, E.; Jansen, M.; Jansen, E.; Will, G. Bestimmung der Kristallstruktur von T- Na_3PO_4 mit Röntgen- und Neutronenpulvertchniken. *Z. Für Krist.* **1990**, *192*, 233–243. [[CrossRef](#)]
20. Newsan, J.M.; Cheetham, A.K.; Tofield, B.C. Structural studies of the high-temperature modifications of sodium and silver orthophosphates, II- Na_3PO_4 and II- Ag_3PO_4 , and of the low-temperature form I- Ag_3PO_4 . *Solid State Ion.* **1980**, *1*, 377–393. [[CrossRef](#)]
21. Kizilyalli, M.; Welch, A.J.E. Preparation and X-ray powder diffraction data for anhydrous sodium orthophosphates. *J. Inorg. Nucl. Chem.* **1976**, *38*, 1237–1240. [[CrossRef](#)]
22. Berthet, G.; Joubert, J.C.; Bertaut, E.F. Vacancies ordering in new metastable orthophosphates $[\text{Co}_3\Box]\text{P}_2\text{O}_8$ and $[\text{Mg}_3\Box]\text{P}_2\text{O}_8$ with olivin-related structure. *Z. Für Krist.* **1972**, *136*, 98–105. [[CrossRef](#)]
23. Nord, A.G.; Kierkegaard, P. The crystal structure of $\text{Mg}_3(\text{PO}_4)_2$. *Acta Chem. Scand.* **1968**, *22*, 1466–1474. [[CrossRef](#)]
24. Baykal, A.; Kizilyalli, M.; Kniep, R. Synthesis and Characterisation of Anhydrous Magnesium Phosphate $\text{Mg}_3(\text{PO}_4)_2$. *Turk. J. Chem.* **1997**, *21*, 394–400.
25. Nord, A.G.; Stefanidis, T. The cation distribution between five- and six-coordinated sites in some $(\text{Mg}, \text{Me})_3(\text{PO}_4)_2$ solid solutions. *Mater. Res. Bull.* **1980**, *15*, 1183–1191. [[CrossRef](#)]
26. Jaulmes, S.; Elfakir, A.; Quarton, M.; Brunet, F.; Chopin, C. Structure cristalline de la phase haute température et haute pression de $\text{Mg}_3(\text{PO}_4)_2$. *J. Solid State Chem.* **1997**, *129*, 341–345. [[CrossRef](#)]
27. Lukaszewicz, K. Crystal structure of alpha- $\text{Mg}_2\text{P}_2\text{O}_7$ and the mechanism of phase transition beta->alpha- $\text{Mg}_2\text{P}_2\text{O}_7$. *Bull. Acad. Pol. Sci., Ser. Sci. Chim.* **1967**, *15*, 53–57.
28. Datars, W.R. ESR Study of Mn^{2+} in α - and β - $\text{Mg}_2\text{P}_2\text{O}_7$. *J. Chem. Phys.* **1967**, *46*, 796–803.
29. Beucher, M.; Grenier, J.C. Données cristallographiques sur les tetrametaphosphates du type $\text{MII}_2\text{P}_4\text{O}_{12}$ (MII=Ni, Mg, Zn, Cu, Co, Mn). *Mater. Res. Bull.* **1968**, *3*, 643–647. [[CrossRef](#)]
30. Nord, A.G.; Lindberg, K.B. The Crystal Structure of Magnesium Tetrametaphosphate, $\text{Mg}_2\text{P}_4\text{O}_{12}$. *Acta Chem. Scand.* **1975**, *29*, 1–6. [[CrossRef](#)]
31. Stachel, D.; Paulus, H.; Guenter, C.; Fuess, H. Crystal structure of magnesium ultraphosphate, $\text{MgP}_4\text{O}_{11}$. *Z. Für Krist.* **1992**, *199*, 275–276. [[CrossRef](#)]
32. Meyer, K.; Hobert, H.; Barz, A.; Stachel, D. Infrared spectra and structure of various crystalline ultraphosphates and their glasses. *Vib. Spectrosc.* **1994**, *6*, 323–332. [[CrossRef](#)]
33. Yakubovich, O.V.; Dimitrova, O.V.; Vidrevich, A.I. Magnesium ultraphosphate $\text{MgP}_4\text{O}_{11}$: Growth and crystal structure. *Crystallogr. Rep.* **1993**, *38*, 176–180.
34. Partridge, E.P.; Hicks, V.; Smith, G.W. A Thermal, Microscopic and X-Ray Study of the System NaPO_3 - $\text{Na}_4\text{P}_2\text{O}_7$ ¹. *J. Am. Chem. Soc.* **1941**, *63*, 454–466. [[CrossRef](#)]
35. Morey, G.W.; Ingerson, E. The binary system NaPO_3 - $\text{Na}_4\text{P}_2\text{O}_7$. *Am. J. Sci.* **1944**, *242*, 1–6. [[CrossRef](#)]
36. Turkdogan, E.T. Phase Equilibrium Investigation of the Na_2O - P_2O_5 - SiO_2 Ternary System. *J. Iron Steel Inst. Lond.* **1952**, *172*, 1–15.
37. Markina, I.B.; Voskresenskaya, N.K. Fusibility of a mutual system of sodium and potassium meta- and orthophosphates. *Russ. J. Inorg. Chem.* **1969**, *14*, 1188–1192.
38. Osterheld, R.K.; Bahr, E.W. Liquidus diagram for the sodium orthophosphate-sodium pyrophosphate system. *J. Inorg. Nucl. Chem.* **1970**, *32*, 2539–2541. [[CrossRef](#)]
39. Berak, J.; Znamierowska, T. Phase equilibria in the system CaO - Na_2O - P_2O_5 . Part II. The partial system $\text{Ca}(\text{PO}_3)_2$ - Na_2O - P_2O_5 . *Rocz. Chem.* **1972**, *46*, 1697–1708.
40. Mixer, W.G. ART. XII-The Heat of Formation of Trisodium Ortho phosphate, Trisodium Orthoarsenate, the Oxides of Antimony, Bismuth Trioxide; and fourth paper on the Heat of Combination of Acidic Oxides with Sodium Oxide. *Am. J. Sci.* **1909**, *28*, 103–111. [[CrossRef](#)]
41. Irving, R.J.; McKerrell, H. Standard heats of formation of NaH_2PO_4 , Na_2HPO_4 and Na_3PO_4 . *Trans. Faraday Soc.* **1967**, *63*, 2913–2916. [[CrossRef](#)]
42. Irving, R.J.; McKerrell, H. Standard heats of formation of two sodium pyrophosphates, sodium trimetaphosphate, and sodium tetrametaphosphate. *Trans. Faraday Soc.* **1968**, *64*, 879–882. [[CrossRef](#)]
43. Irving, R.J.; McKerrell, H. Standard heats of formation of the sodium triphosphates $\text{Na}_5\text{P}_3\text{O}_{10}(\text{cI})$, $\text{Na}_5\text{P}_3\text{O}_{10}(\text{cII})$ and $\text{Na}_5\text{P}_3\text{O}_{10} \cdot 6\text{H}_2\text{O}(\text{c})$. *Trans. Faraday Soc.* **1968**, *64*, 875–878. [[CrossRef](#)]
44. Krivtsov, N.V.; Titova, K.V.; Rosolovskii, V.Y. The Enthalpy of Dissolution and Standard Enthalpy of Formation of Sodium Pyrophosphate Peroxosolvate $\text{Na}_4\text{P}_2\text{O}_7 \cdot 3\text{H}_2\text{O}_2$. *Russ. J. Inorg. Chem.* **1995**, *40*, 603–605.

45. Zhuang, W.; Liang, J.; Qiao, Z.; Shen, J.; Shi, Y.; Rao, G. Estimation of the standard enthalpy of formation of double oxide. *J. Alloys Compd.* **1998**, *267*, 6–10. [[CrossRef](#)]
46. Khaled, H.G.B.; Khattech, I.; Jemal, M. Standard enthalpy of formation of disodium hydrogen phosphate hexahydrate and sodium diphosphate. *J. Chem. Thermodyn.* **2011**, *43*, 521–526. [[CrossRef](#)]
47. Andon, R.J.L.; Counsell, J.F.; Martin, J.F.; Mash, C.J. Thermodynamic properties of phosphorus compounds. II. Low-temperature heat capacity and entropy of sodium mono-, di-, and tri-phosphates. *J. Appl. Chem.* **1967**, *17*, 65–70. [[CrossRef](#)]
48. Ashcroft, S.J.; Keen, E.; Mortimer, C.T. Thermochemistry of formation of sodium polyphosphates from sodium orthophosphates. *Trans. Faraday Soc.* **1969**, *65*, 2851–2855. [[CrossRef](#)]
49. Lazarev, V.B.; Sokolova, I.D.; Sharpataya, G.A. DSC study of polymorphism of $\text{Na}_4\text{P}_2\text{O}_7$. *Thermochim. Acta* **1985**, *92*, 301–304. [[CrossRef](#)]
50. Grantscharova, E.; Avramov, I.; Gutzow, I. Calorimetric study of vitreous and crystalline sodium metaphosphate NaPO_3 . *Thermochim. Acta* **1986**, *102*, 249–256. [[CrossRef](#)]
51. Berak, J. The system magnesium oxide-phosphorus pentoxide. *Rocz. Chem.* **1958**, *32*, 17–22.
52. Bobrownicki, W.; Slawski, K. Pseudobinary section $\text{Ca}_3(\text{PO}_4)_2\text{-Mg}_3(\text{PO}_4)_2$ in the ternary system $\text{CaO-MgO-P}_2\text{O}_5$. *Rocz. Chem.* **1959**, *33*, 251–254.
53. Czupinska, G. The system $\text{YPO}_4\text{-Mg}_3(\text{PO}_4)_2\text{-Mg}_2\text{P}_2\text{O}_7$. *J. Therm. Anal.* **1992**, *38*, 2343–2347. [[CrossRef](#)]
54. Oetting, F.L.; McDonald, R.A. The thermodynamic properties of magnesium orthophosphate and magnesium pyrophosphate. *J. Phys. Chem.* **1963**, *67*, 2737–2743. [[CrossRef](#)]
55. Bookey, J.B. The free energy of formation of magnesium phosphate. *J. Iron Steel Inst. Lond.* **1952**, *172*, 66–68.
56. Roy, R.; Middleswarth, E.T.; Hummel, F.A. Mineralogy and thermal behavior of phosphates; I. Magnesium pyrophosphate. *Am. Mineral.* **1948**, *33*, 458–471.
57. Calvo, C. The crystal structure of $\alpha\text{-Mg}_2\text{P}_2\text{O}_7$. *Acta Crystallogr.* **1967**, *23*, 289–295. [[CrossRef](#)]
58. Rakotomahanina-Rolaisoa, E.; Henry, Y.; Durif, A. Phase equilibrium diagram for $\text{TiPO}_3\text{-Co}(\text{PO}_3)_2$, $\text{TiPO}_3\text{-Mg}(\text{PO}_3)_2$, and $\text{TiPO}_3\text{-Ca}(\text{PO}_3)_2$. *Bull. Soc. Fr. Mineral. Cristallogr.* **1970**, *93*, 43–51.
59. Berthelot, M. *Thermochimie: Données et Lois Numériques*; Gauthier-Villars: Paris, France, 1897.
60. Stevens, C.G.; Turkdogan, E.T. The heats of formation of trimanganous phosphate and trimagnesium phosphate. *Trans. Faraday Soc.* **1954**, *50*, 370–373. [[CrossRef](#)]
61. Lopatin, S.I.; Semenov, G.A.; Kutuzova, Y.L.A. A mass-spectrometric investigation of the thermal dissociation of condensed magnesium phosphates. *Inorg. Mater.* **1986**, *22*, 1320–1323.
62. Lopatin, S.I.; Semenov, G.A. A Mass-spectrometric investigation of thermal dissociation of alkaline earth metal monophosphates. *Neorg. Mater.* **1989**, *25*, 645–650.
63. Abdelkader, S.B.; Cherifa, A.B.; Khattech, I.; Jemal, M. Synthèse, caractérisation et thermochimie du phosphate trimagnésien et du phosphate tricalcique. *Thermochim. Acta* **1999**, *334*, 123–129. [[CrossRef](#)]
64. Iwase, M.; Akizuki, H.; Fujiwara, H.; Ichise, E.; Yamada, N. A thermodynamic study of $\text{MgO-P}_2\text{O}_5$ slags by means of solid-oxide galvanic cell at 1673K. *Steel Res.* **1987**, *58*, 215–219. [[CrossRef](#)]
65. Jung, I.H.; Hudon, P. Thermodynamic Assessment of P_2O_5 . *J. Am. Ceram. Soc.* **2012**, *95*, 3665–3672. [[CrossRef](#)]
66. Wu, P.; Eriksson, G.; Pelton, A.D. Optimization of the thermodynamic properties and phase diagrams of the $\text{Na}_2\text{O-SiO}_2$ and $\text{K}_2\text{O-SiO}_2$ systems. *J. Am. Ceram. Soc.* **1993**, *76*, 2059–2064. [[CrossRef](#)]
67. Mao, H.; Selleby, M.; Sundman, B. A re-evaluation of the liquid phases in the $\text{CaO-Al}_2\text{O}_3$ and $\text{MgO-Al}_2\text{O}_3$ systems. *Calphad* **2004**, *28*, 307–312. [[CrossRef](#)]

Disclaimer/Publisher’s Note: The statements, opinions and data contained in all publications are solely those of the individual author(s) and contributor(s) and not of MDPI and/or the editor(s). MDPI and/or the editor(s) disclaim responsibility for any injury to people or property resulting from any ideas, methods, instructions or products referred to in the content.